AIAA JOURNAL
Vol. 46, No. 1, January 2008

Flowfield Characteristics of a Confined Transverse Slot Jet

K. A. Ahmed,* D. J. Forliti,† J. K. Moody,* and R. Yamanaka*
The State University of New York at Buffalo, Buffalo, New York 14260

DOI: 10.2514/1.29799

The current study explored the mean and turbulent flowfield features of a confined transverse slot jet. The slot jet spans 95% of the full channel spanwise dimension, a geometrical feature found to result in a highly three-dimensional mean flowfield. The transverse slot jet produces a recirculation bubble that has similarities to that found for the flow downstream of a rearward-facing step. The flowfield results were compared with a 2:1 expansion ratio step flow and the observations were discussed in the context of how the transverse slot jet may provide advantages compared with a sudden expansion for subsonic combustors. High turbulence levels are achieved and large turbulent length scales are produced for strong transverse slot jets. The momentum ratio of the jet to that of the channel is found to be a governing parameter, and the dimensions of the recirculation zone scale with this parameter. A series of models constructed in ANSYS/CFX-10 were done to complement the experimental work and showed that the three-dimensionality of the mean flow disappears when the slot jet extends fully across the channel.

Nomenclature

D	=	jet slot thickness
H	=	channel height
h	=	height of the mean recirculation zone
J	=	momentum flux ratio
l	=	length of the mean recirculation zone
L_{11}	=	integral length scale
r	=	velocity ratio
S_{11}	=	strain rate
U	=	mean streamwise velocity
U_j	=	jet flow velocity
U_o	=	maximum channel flow velocity with no jet flow
u'	=	streamwise velocity fluctuation
v'	=	cross-stream velocity fluctuation
W_j	=	slot jet width
W_o	=	channel width
w'	=	spanwise velocity fluctuation
x	=	streamwise coordinate
y	=	cross-stream coordinate
z	=	spanwise coordinate
ρ_j	=	slot jet density
ρ_o	=	channel flow density

I. Introduction

THE jet issuing into a crossflow stream, or the transverse jet, has received extensive attention from the fluid dynamics research community, both as a practical configuration found in numerous engineering applications and as a fundamental three-dimensional turbulent shear flow suitable for validating turbulent flow models. The nonreacting transverse jet is a configuration applicable for chimney stacks, V/STOL aircraft, dilution of combustion gases in gas turbines, and film cooling. Reacting transverse jets include the flame stabilization of a fuel jet issuing into crossflow as a model of stack flares and secondary combustion zones in gas turbine combustion chambers. Many previous efforts focused on the detailed flowfield features, dimensionless groupings, streamwise trajectory behavior, and scaling properties of round jets issuing into unconfined crossflow [1–11]. Vorticity dynamics have played an important role in many studies, with emphasis on the origin and dynamics of the counter-rotating vortex pair (CVP) [10,12–18]. Other vortex systems present in the round transverse jet include the horseshoe vortex formed upstream of the jet, the jet shear layer structure, and the wake vortices that occur downstream of the jet for sufficiently strong jet-to-crossflow velocity ratios. For experimental studies, flow visualization of this highly three-dimensional flow has been an invaluable tool [19–23].

Alternative jet nozzle shapes have also received attention to explore a passive means for mixing enhancement for transverse jets [24–29]. Confinement has also been considered, related primarily to gas turbine combustors [30]. The confined transverse slot jet in a rectangular duct has received less attention, although a small number of studies have been conducted [31–35]. These efforts considered a slot jet that spans the entire dimension of the confinement (i.e., channel), and results show that the generated flowfield is nominally two-dimensional with respect to mean and turbulence statistics. It is not clear whether there is any CVP-type structure found for these confined transverse slot jet cases. A recent study by Plesniak and Cusano [36] explored the flowfield created for a rectangular jet issuing into a confined crossflow, in which the width of the jet was less than the depth of the crossflow duct. This study showed that a CVP was established under most conditions with a slot jet that spanned 80% of the duct depth.

The stabilization of nonpremixed combustion using transverse injection has also been studied. Kalghatgi [37] explored the stabilization of round jet flames exposed to crossflow and provided an empirical relation that predicted the stabilization limit for a variety of jet fuels. Fuel or air injected normal to a supersonic cross stream, relevant for scramjet flows, has been employed in conjunction with cavities and steps to enhance flame anchoring in the supersonic environment [38,39].

Ramjet propulsion systems rely on low-speed recirculation regions for flame anchoring [40]. Sudden flow path expansions, either using rearward-facing steps or bluff bodies, are employed to anchor the flame and produce turbulence that facilitates efficient volumetric combustion rates. An asymmetric rearward-facing step flow shown in Fig. 1a illustrates the features of the separated flow that are used for flame anchoring and production of turbulence for efficient combustion. The internal surfaces of the engine that have area projections in the streamwise direction are responsible for thrust production. The downstream-facing surface area at the expansion plane projects in the streamwise direction; hence, the pressure along this surface is a primary source of thrust. Although thrust may be produced with a sudden expansion geometry, the pressure at the dump plane is lower than in the downstream region in which partial

Received 16 January 2007; accepted for publication 4 September 2007.

*Research Assistant, Department of Mechanical and Aerospace Engineering, 311 Jarvis Hall. Student Member AIAA.

†Assistant Professor, Department of Mechanical and Aerospace Engineering, 326 Jarvis Hall. Member AIAA.

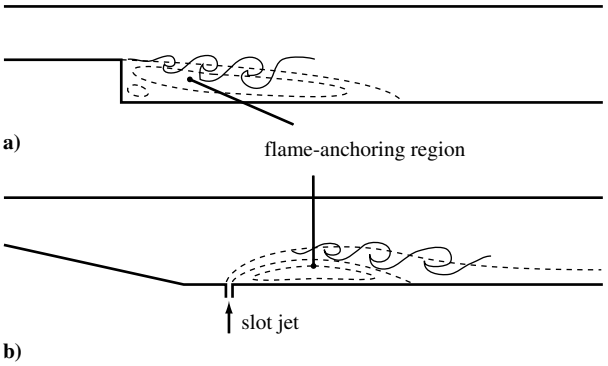

Fig. 1 Schematic of a) the rearward-facing step and b) the transverse-slot-jet-based ramjet combustor.

static pressure recovery is achieved. Hence, the step geometry has an associated drag penalty. Additionally, the impedance associated with a sudden area change in a duct often participates in thermoacoustic combustion instabilities [41,42].

Figure 1b shows an alternative ramjet combustor, the dump plane of which is replaced by an asymmetric diffuser that efficiently recovers dynamic pressure through avoiding flow separation. The diffuser has the same streamwise projected area as the step configuration shown in Fig. 1a. For the same operating conditions, the diffuser geometry will result in higher thrust due to the increase in pressure along the diffuser. Although the diffuser increases thrust, the flame-anchoring and turbulence-production traits of the recirculation zone are lost. A fluidic-based scheme is proposed to induce a large-scale recirculation zone that will provide the necessary environment for flame stabilization and efficient combustion rates. A single slot jet issuing into a rectangular channel is known to produce a global recirculation zone that is reminiscent of the flow produced downstream of a rearward-facing step [31]. The long-range objective of the current research project is to study the combustion characteristics of a ramjet model that employs a transverse slot jet for stabilizing the flame and producing highly turbulent flames, with the motivation of increasing thrust due to the higher loads on the diffuser in comparison with a rearward-facing step. The present paper describes the nonreacting studies that focus on understanding the mean and turbulent flow characteristics of the recirculation zone created using a transverse slot jet. Comparisons are made to an analogous rearward-facing step flow. The results support the proposal that such a fluidic approach has potential for flame stabilization and combustion rate enhancement.

II. Experimental Setup

The experiments were conducted in the Combustion Laboratory in the Mechanical and Aerospace Engineering Department at The State University of New York at Buffalo. The experimental facility is shown in Fig. 2. A channel flow facility was constructed having a short dimension height of 12.5 mm and an aspect ratio of 4:1. The air

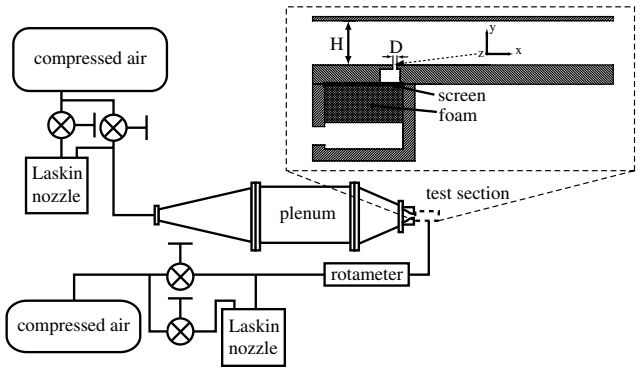

Fig. 2 Experimental facility and test section.

for the main channel flow is generated using a blowdown type facility, in which pressurized air is regulated and metered before delivery to the plenum of the channel flow facility. The plenum contains flow conditioning in the form of two coarse screens, a 1-in. section of 1/8-in. aluminum honeycomb, followed by two fine-mesh screens. The Reynolds number based on the channel velocity U_o and channel height H was held constant at approximately 19,000.

The details of the test section are shown in Fig. 2. An injection slot is situated on the bottom wall of the test channel. The slot spans 95% of the full channel spanwise depth and is centered in the spanwise direction. The slot jet has a short dimension of 1.2 mm. Compressed air was first passed through a Laskin nozzle for seeding the airstream with nominally 1-μm-diam olive-oil droplets before delivery to the manifold for the injection flow [43]. High-porosity open-cell foam and a screen were used in the jet manifold to establish spanwise uniform flow through the slot jet. The foam filled the cross section of the manifold plenum and was 10 mm in thickness. Bypass air around the Laskin nozzle was used to control the seeding rate for a fixed flow rate to match the particle seeding density of the crossflow stream. The injection air was metered using Dwyer rotameters employing corrections for deviations from standard density. The channel flow rate was set using digital particle image velocimetry (DPIV) before each experiment.

DPIV was used to study the velocity field of the transverse slot jet flowfield. The system is controlled by IDT software ProVISION-XS, which employs a PC and an IDT MotionPro X Timing Hub for synchronization. A New Wave Research Solo PIV III Nd:YAG laser capable of 50 mJ/pulse (532 nm) at 15 Hz is used as a light source. An X-Stream VISION camera is used for collecting images for cross-correlation-mode DPIV. Sheet-forming optics and a 45-deg mirror are used to deliver an approximately 1-mm-thick light sheet to the test section. DPIV data were collected in the side and plan views of the transverse slot jet; different DPIV planes are taken through proper orientation of the experiment relative to the laser sheet. Images were processed using 32×32 pixel interrogation regions with 50% overlap, resulting in a spatial resolution of 0.64 mm. Subpixel displacement calculations are done using a true resolution algorithm [44].

Generally, 800 image pairs were collected for each case. Uncertainty due to precision and bias error (due to peak locking) for instantaneous vector calculations was approximately 0.016 and 0.02 pixels, respectively. Uncertainties due to flow unsteadiness over time and calibration of the DPIV were checked using overlapping regions for different camera locations with data taken during different times during the same experiment. Uncertainty estimates for the mean and rms fluctuating velocity, based on Student's t- and chi-squared distributions, were found to be 3 and 2% of U_o, respectively. Note that the uncertainty of the rms fluctuating velocity is approximately 5% of the peak rms fluctuation velocity ($\sim$12 m/s). The uncertainty of the Reynolds stress was estimated to be approximately 20% in the high-turbulence region, based on data from 30 sets of 812 vector fields for a related experiment with similar turbulence intensities. The uncertainty in the strain rates was found experimentally to be approximately 7% of the peak value ($\sim$8000 1/s). Figure 3 shows comparisons of sample cross-stream profiles of various velocity statistics for two sets of 400 samples. The comparison of the two data sets with reference to the included error bars (based on 400 samples instead of 800) show that the scatter is within the estimated uncertainty. All uncertainties are plus and minus the stated value.

Figure 4 shows profiles of the mean and rms fluctuation of the streamwise velocity across the channel near the injection location with no injection flow. The channel flow has a low turbulence level in the central part, bounded by turbulent boundary layers near the channel walls. The boundary-layer thickness δ_{99} is approximately 1.9 mm. The velocities are normalized by the maximum channel flow velocity with no jet flow, U_o. The velocity profile of the injection jet is expected to play a role in the transverse slot jet flowfield. Experimental results on round jets in crossflow show that top-hat profiles produce stronger vortex structure and bend earlier than a fully developed jet profile [11,45,46]. The jet orifice for the current

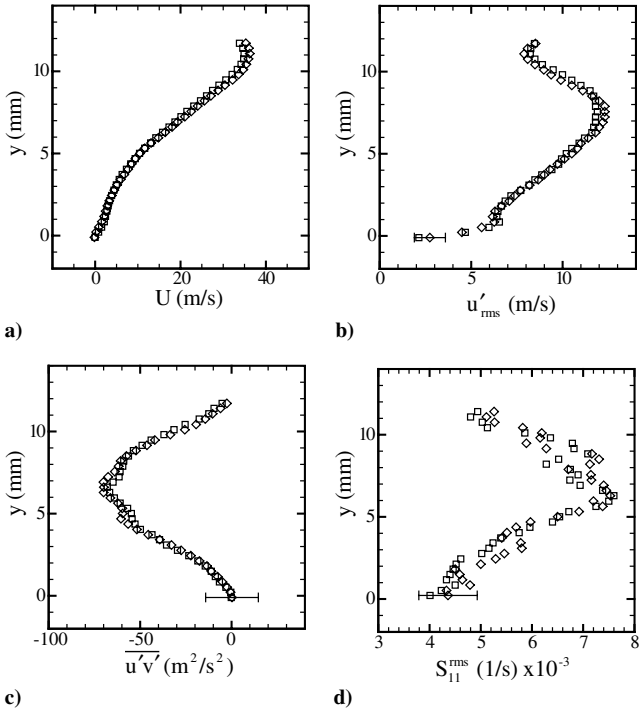

Fig. 3 Repeatability of a) mean velocity, b) rms streamwise fluctuation, c) Reynolds shear stress, and d) rms strain rate.

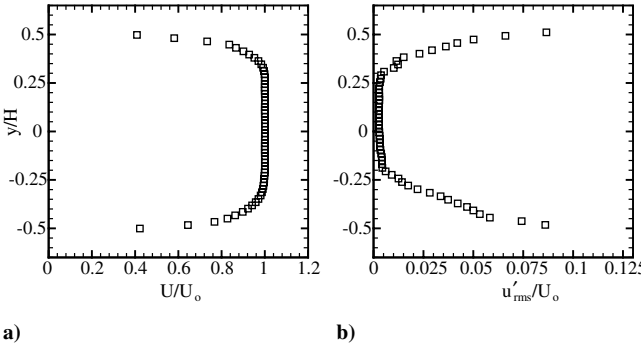

Fig. 4 Profiles of a) mean streamwise velocity and b) rms of streamwise velocity fluctuation for the channel flow without the transverse jet.

experiment is short (L/D is on the order of unity), and the velocity profile is expected to have a nominally top-hat shape.

In addition to the transverse slot jet, a 2:1 area ratio rearward-facing step-flow case was studied through employment of a leading-edge contoured step insert piece in the channel section. The data in this case were in strong agreement with the step-flow results of Forliti and Strykowski [47]; hence, limited data for this case will be presented. The step flow provides a benchmark for the transverse slot jet flowfield.

A numerical component for the current project was conducted using ANSYS/CFX-10. A three-dimensional grid was generated to match the injection and channel dimensions. Figure 5 shows the computational domain for the three-dimensional RANS calculation. The standard k-ε model was used. The purpose of the numerical study was to determine the qualitative effect of the ratio of the slot jet to channel width as well as to help explain some of the experimental observations. Comparisons between the numerical and experimental results will be discussed in the following section. A uniform crossflow was employed for the channel flow inlet, and no-slip boundary conditions were used on all wetted surfaces. The slot jet was modeled as uniform flow and was applied on the slot passage located one channel height H upstream to allow interactions between the crossflow and the jet flow upstream of the slot jet exit [1,2,20,21,46]. The slot injection was located five channel heights downstream of the inflow boundary to allow boundary-layer growth on the channel wall, matching the boundary-layer thickness of the experiments. Two slot widths were considered: one case with a 95% slot width matching the experiment and one case with a 100% slot width that matches much of the other confined slot jet in crossflow cases from literature.

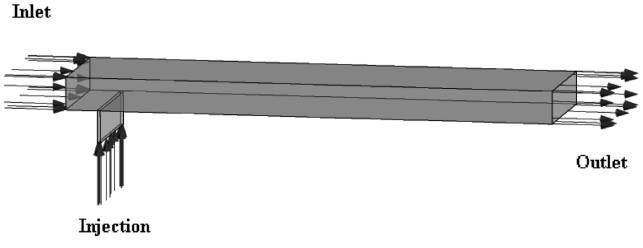

Fig. 5 CFD model for the transverse slot jet.

III. Results

The primary motivation of the present work was to study the characteristics of the recirculation zone induced using a transverse slot jet and to analyze the results in the context of potential for flame holding and turbulent combustion. A parameter used to characterize the jet in crossflow configuration is the momentum flux ratio, defined as

$$J = \frac{\rho_j U_j^2}{\rho_o U_o^2} \tag{1}$$

where ρ is the density, U is the characteristic velocity, and the subscripts j and o represent the jet and crossflow, respectively. The square root of the momentum flux ratio r is the equivalent velocity ratio [9]. The definition of the jet velocity becomes subjective, because the jet always has a velocity profile that is not perfectly uniform. A bulk- or mass-flow-averaged velocity is often used, although others have used a definition that is more akin to a momentum-based average value. It has been shown that the jet trajectory normalized by the jet diameter D is a function of the velocity ratio r, although normalization by rD typically results in a collapse of profiles over a range of velocity ratios [9,12]. Jet initial conditions and Reynolds number effects are responsible for the observed scatter between different experimental configurations [23,48]. For the present work under confined conditions, the channel height H is a relevant length scale, because the objective of the design is to induce a global recirculation zone that will scale with the channel dimension. Because of this, the momentum ratio (MR) of the jet to the channel flow is expected to be a more appropriate parameter and is defined as

$$\mathrm{MR} = \frac{\rho_j U_j^2 D W_j}{\rho_o U_o^2 H W_o} \tag{2}$$

where W is the width of the slot or channel. Results to be presented elsewhere using a different slot jet diameter D have shown that the recirculation bubble dimensions scale predominantly with MR and not J.

Figure 6 shows two sample instantaneous side-view velocity-vector fields taken in the midspan plane for a MR $= 0.12$ ($J = 1.24$). The mass flow ratio of the jet to the channel flow is 0.1. The spatial resolution of the DPIV data is marginal near the injection point at which the slot jet is only represented by a few velocity vectors. The transverse jet penetrates into the crossflow, causing the formation of relatively large turbulent structures that scale with the penetration height. There is a region above the jet near the streamwise injection point in which the crossflow locally accelerates as it encounters the blockage caused by the transverse jet. The flow on the upper half of the channel flow is nominally undisturbed.

Two instantaneous velocity-vector fields for a higher MR of 0.49 ($J = 5.28$) are shown in Fig. 7. The mass flow ratio for this case is

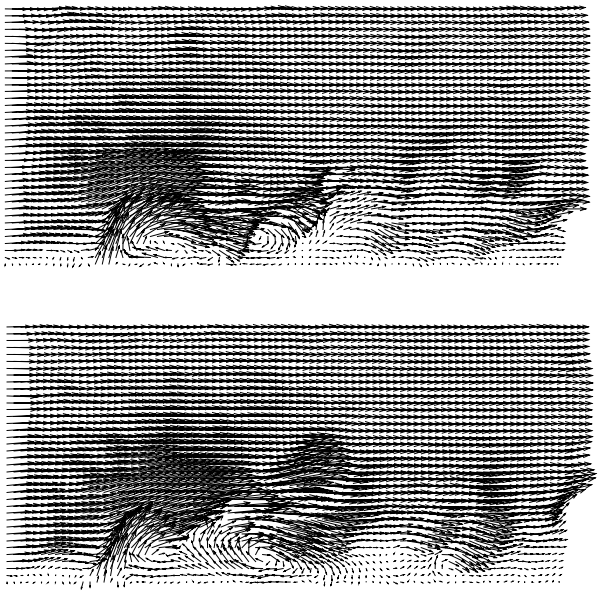

Fig. 6 Instantaneous velocity vectors for MR = 0.12.

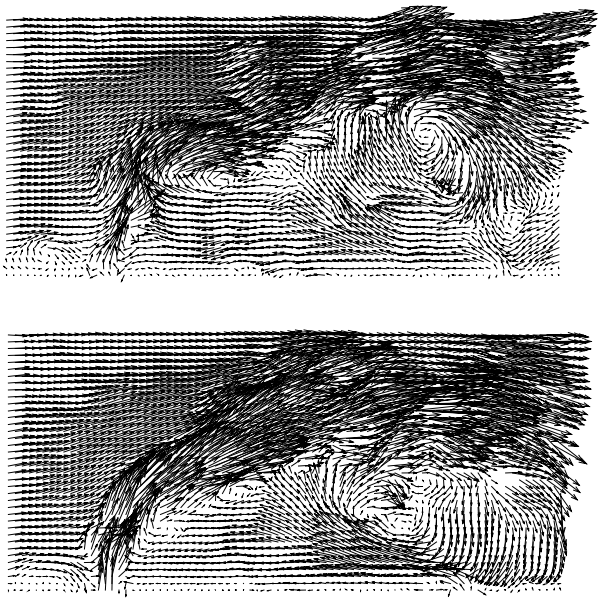

Fig. 7 Instantaneous velocity vectors for MR = 0.49.

0.22. The jet appears to penetrate all the way across the channel, although entrainment of crossflow occurs along the trajectory. Acceleration and turning of the crossflow is again observed above the deflected jet. Large vortical structures are also observed, and large regions of instantaneous reverse flow are present downstream of the injection location.

The mean streamline pattern is shown in Fig. 8 for the MR cases of 0.12 and 0.49. The streamline patterns show that the transverse slot jet induces a recirculation zone reminiscent of that produced due to a sudden expansion (e.g., the flow downstream of a rearward-facing step). This is one of the important flow features required for flame stabilization in a high-speed reacting flow. Note that due to the large length of the recirculation bubble for the higher-MR case, multiple camera locations were required. The camera was moved during the experiment, recalibrated, and 800 image pairs were collected at each camera location. The slightly overlapping data regions were patched together to obtain the overall domain. The streamline pattern provides a means for defining the dimensions of the recirculation zone, which are relevant when considering the dynamics of the flame stabilization process [49]. The height and length of the recirculation

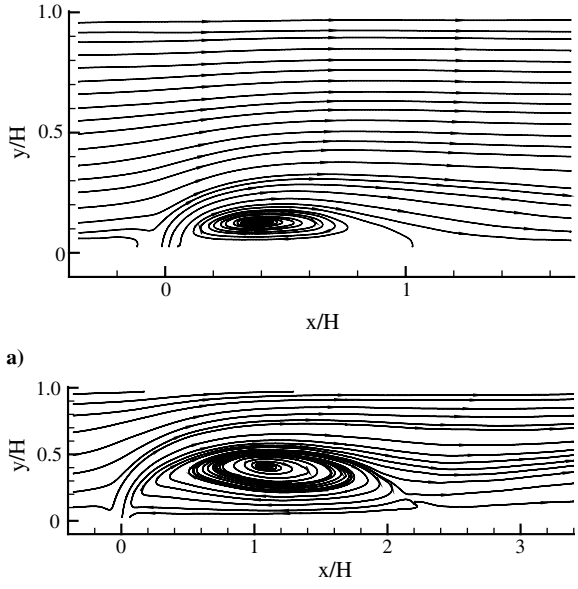

Fig. 8 Mean streamline pattern for MR of a) 0.12 and b) 0.49.

are determined using the streamline that is attached to the downstream edge of the injection slot; for two-dimensional flow, this streamline establishes an attachment point at the downstream end of the confined recirculation zone. Such a streamline appears to exist for the low-momentum-ratio case, whereas for the high-momentum-ratio case the streamline along the trailing edge of the recirculation bubble has a bifurcating characteristic that indicates the presence of mean flow three-dimensionality [50]. The length-to-height ratio of the recirculation bubble is in the range of three to four, whereas for the 2:1 area ratio step flow, the ratio is on the order of 7 [47,51]; hence, the transverse jet produces a much more compact recirculation zone. Additionally, the rearward-facing step flow contains a small secondary recirculation zone near the dump plane that is not present for the transverse slot jet flowfields [47].

The mean streamwise velocity distributions for the two cases are shown in Fig. 9. The velocity component is normalized by the maximum channel velocity without injection, U_o, which was nominally 26 m/s. The low-momentum-ratio case shows a slight

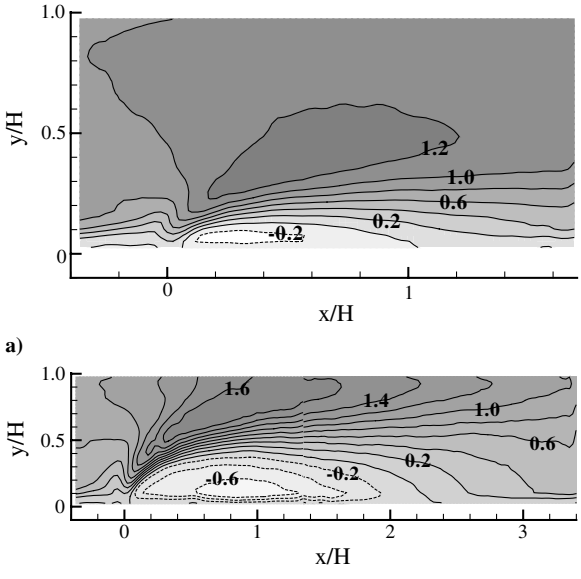

Fig. 9 Mean streamwise velocity distributions for MR of a) 0.12 and b) 0.49.

acceleration of the main channel flow due to the blockage created by the transverse jet. The reverse velocity in the recirculation zone reaches approximately 20% of the channel characteristic velocity. The acceleration and reverse flow both increase with increasing MR. At MR = 0.49, the peak velocity difference across the channel in the region of the recirculation region is nominally 2.2 times the characteristic velocity, providing a large shear magnitude for turbulence production that will be beneficial for volumetrically efficient turbulent combustion. The peak shear was nominally the same for the 2:1 rearward-facing step flow. The transverse jet acts as a virtual nozzle for the channel flow (i.e., causes a contraction of the crossflow). The turbulence of the slot jet must also play a role, either as the initial turbulence that grows in the mean shear, or act as a disturbance to the unstable separated channel flow. One might expect that the high reverse velocities may be detrimental to flame holding, because the residence time of a typical reactant pocket may be too short for combustion to be completed, although this may be alleviated if the turbulent flame speed within the recirculation zone increases. The high-momentum-ratio case provides a nominal 50% contraction of the channel flow (as indicated in Fig. 8). The slight discontinuity in the isovelocity lines near the middle of Fig. 9b is caused by uncertainties in the mean velocity and image window locations. The low-MR case was found to satisfy two-dimensional mass conservation, whereas the higher-MR case did not, suggesting the presence of out-of-plane motion. The rearward-facing step flow also contains a nominally stagnant region in the first couple of step heights downstream of the step in which the recirculation velocities are very low. The stagnation region near the dump plane for the step flow has less shear than the downstream region, rendering the upstream region less effective at producing turbulent energy [47].

The normalized turbulence levels are defined as

$$\frac{\left(u'^2_{\text{rms}} + v'^2_{\text{rms}}\right)^{1/2}}{U_o} \tag{3}$$

where u' and v' are the streamwise and cross-stream velocity fluctuations, and rms represents a root mean square. Figure 10 shows the normalized turbulence levels for the two MR cases. For the low-MR case, the injection creates a highly turbulent flow that remains near the injection wall, with nonturbulent crossflow flowing above the turbulent region. For the higher-MR case shown in Fig. 10b, the turbulence levels are much higher and span the entire height of the channel. In fact, the peak-turbulence contour is slightly skewed toward the upper wall in the downstream half of the domain. The high turbulence levels begin to decrease in the downstream half of the domain. Reduced turbulent energy production caused by a drop in mean shear as well as dissipation, convection, and diffusion of turbulent energy is responsible for the reduction in peak turbulence levels.

The peak normalized reverse velocity obtained for the step flow of Forliti and Strykowski [47] was 0.4 (when scaled with the equivalent characteristic velocity), whereas the MR = 0.49 case value is 0.6. Likewise, the peak turbulence level for the step-flow case was nominally 0.4, whereas the peak turbulence level for the current study is 0.6, representing a 50% increase in turbulence level using a transverse slot jet compared with the step flow. Additionally, the step-flow configuration requires several channel heights of development before peak turbulence levels are reached, whereas the transverse slot jet quickly acquires high turbulence levels due to the increased shear and potential effects of the jet turbulence. The comparison between the current results and the step flow indicate a potentially significant improvement for premixed combustion systems using transverse slot jets. Note that although it is unclear whether higher levels of reverse flow will have a positive effect on flame anchoring, results for a dump combustor with counterflow control suggest that a smaller recirculation zone with high reverse-flow velocities may indeed improve flame holding [52–54].

Figure 11 presents the normalized Reynolds stress term $\overline{u'v'}/U_o^2$ for the two MR cases. The poor spatial resolution of the near field of the slot jet results in unresolved Reynolds stresses. The downstream region shows the development of Reynolds stress as the structures grow to sufficient size to be resolved by DPIV. The Reynolds stresses increase dramatically as the momentum ratio increases, increasing by a factor of 5 between the two cases. For reference, the normalized peak Reynolds stress measured in the present study for a rearward-facing step flow was approximately −0.045 compared with −0.15 for the high-momentum-ratio transverse slot jet. The results suggest that the turbulent energy production is very high for the high-momentum-ratio case and will produce higher turbulence levels than the rearward-facing step flow having the same mean shear. The high relative uncertainty of 20% for the Reynolds shear stress is small relative to the noted difference between the slot jet and the rearward-facing step.

Strain rates are very important for combustion. Premixed flames exposed to excessive strain rates result in reduced turbulent flame speeds and local/global extinction [55,56]. The DPIV diagnostic spatially filters the velocity field, equivalent to a low-pass filter in wave-number space. The current spatial resolution is not sufficient to measure dissipation scales; hence, filtering is significant. The strain rate measurements still provide insight for combustion-related strain, because extinction processes are associated with scales that are of the

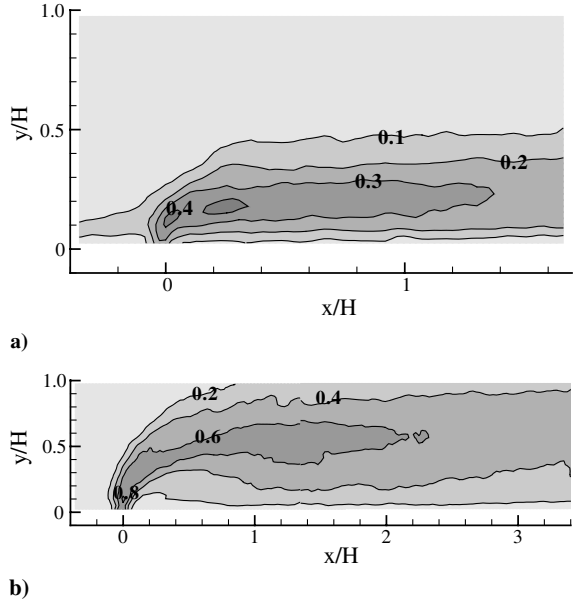

Fig. 10 Normalized turbulence levels for MR of a) 0.12 and b) 0.49.

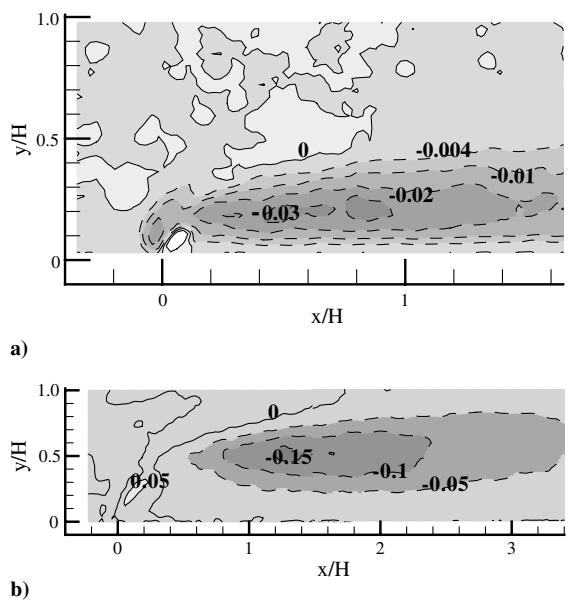

Fig. 11 Reynolds stress for MR of a) 0.12 and b) 0.49.

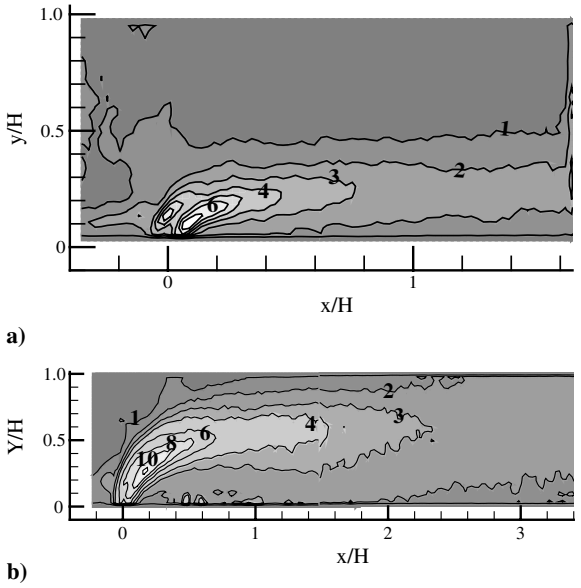

Fig. 12 Strain rates for MR of a) 0.12 and b) 0.49.

same order of magnitude as the flame thickness [57]. Figure 12 presents the normalized rms of the S_{11} component of the strain rate tensor, defined as

$$\frac{S_{11}^{\text{rms}}}{U_o/H} = \frac{[\overline{(\mathrm{d}u/\mathrm{d}x)^2}]^{1/2}}{U_o/H} \tag{4}$$

where $\mathrm{d}u/\mathrm{d}x$ is the instantaneous streamwise velocity gradient in the streamwise direction, and the overbar represents a time average. Note that this definition includes strain due to the mean and fluctuating velocity fields. The strain rate due to mean shear in the streamwise direction is weak except near the injection location (Fig. 9). For the present step-flow results, the normalized rms strain rates achieve a value of approximately two near the downstream half of the recirculation zone. For the low-MR case, the normalized rms strain rates range from two to three over the downstream half of the recirculation bubble, whereas values are slightly higher for the higher-MR case. The results indicate that the transverse jet may be more susceptible to quenching effects under combustion conditions compared with the rearward-facing step, with dependence on the strain rates normalized by the flame strain. Note that under the slot jet trajectory, where flame holding will occur, the rms strain rates are lower than in the peak-turbulence region.

It was shown from the streamline pattern that the flow at the higher MR appeared to contain mean flow three-dimensionality. Spanwise DPIV was conducted by rotating the experiment 90 deg about the streamwise axis, and the measurement plane was adjusted to a number of different locations relative to the plane of the injection wall for the transverse jet. Figure 13 shows the mean streamline pattern in two spanwise planes located at different distances from the injection wall. Note that these are not technically streamlines, because the velocity component out of the plane is generally nonzero. The apparent three-dimensional nature of the flow is readily observed. For the plane closest to the injection wall shown in Fig. 13a, located at $y/H = 0.16$, some interesting features are captured. The crossflow encounters the slot jet and creates a large stagnation point. The crossflow turns toward the side walls on each side of the midspan line and passes through the narrow gap between the slot jet and the side wall. There is a slight asymmetry in the location of the slot jet relative to the channel spanwise center. The asymmetry may be due to actual flow asymmetry that has been observed in round jets in crossflow experiments [9,36] or due to slight misalignment of the light sheet (the light-sheet alignment is accurate to approximately 0.5 mm). Two large-scale vortex structures are observed near the outer edge of the slot jet. Similar structure was observed in the surface streaklines of an unconfined transverse slot jet studied by Krothapalli et al. [24] Fig. 13b shows the spanwise mean streamlines for $y/H = 0.32$ and shows a smaller recirculation region centered in the spanwise plane. A pair of mean flow counter-rotating vortices is also present, although they are located much closer to one another compared with the $y/H = 0.16$ location. The crossflow external to the recirculation region passes around the recirculation bubble in a manner similar to the flow around a smooth obstacle. Such three-dimensionality has not been observed in confined slot jets in which the slot jet spans the entire channel dimension [31,32]. Plesniak and Cusano [36] observed a CVP structure for their slot jet that spanned 80% of the duct depth. Hence, it is expected that the creation of these structures is connected to the fact that the slot jet does not span across the entire channel. This will be discussed in more detail later. The spanwise measurements made in the current study with the 2:1 step flow showed nominal spanwise invariance, although there were some three-dimensional effects near the side walls, as would be expected.

Figure 14 shows the spanwise distribution of the mean streamwise velocity at the two transverse locations. The $y/H = 0.16$ case shown in Fig. 14a shows that the recirculation bubble as defined by the footprint of the zero streamwise velocity contour has a triangular shape, a qualitative feature in agreement with the streamline pattern shown in Fig. 13a. The high mean reverse-velocity region, defined as $U/U_o < -0.4$, is limited to a small region in the center of the span. The region near the side walls contains higher mean streamwise velocities, because the crossflow accelerates as it passes between the slot jet and side wall. The mean streamwise velocity distribution shown in Fig. 14b for $y/H = 0.32$ shows a smaller reverse-flow region. It is clear that the recirculation zone appears to have a domelike shape that is centered in the span and has a peak height in the midspan plane. This shape suggests that the slot jet trajectory has maximum penetration near the spanwise center and a lower trajectory for side-view planes that approach the side walls. This trend is different from previous results for spanwise transverse slot jets under confined conditions in which the slot jet spans the entire channel depth, which has been shown to produce a nominally spanwise uniform flow outside the side-wall boundary layers [31,32]. The vertically oriented high-speed band passing through near $x/H = 0$ in Fig. 14b is the streamwise component of the transverse slot jet that has begun to acquire a streamwise component due to bending by the

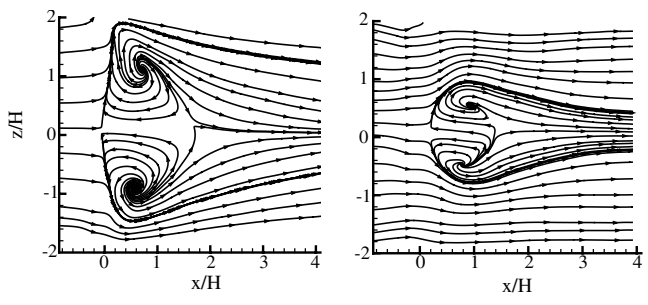

Fig. 13 Mean streamlines in the spanwise plane for y/H of a) 0.16 and b) 0.32.

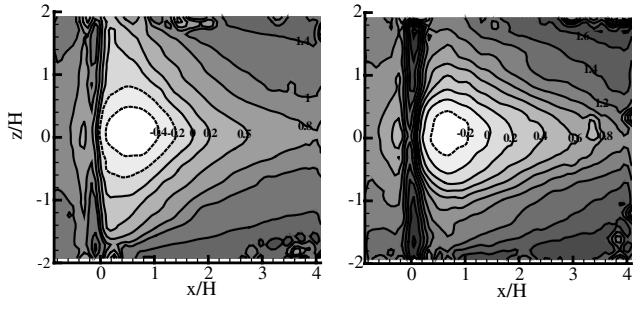

Fig. 14 Distribution of mean streamwise velocity in the spanwise plane for y/H of a) 0.16 and b) 0.32.

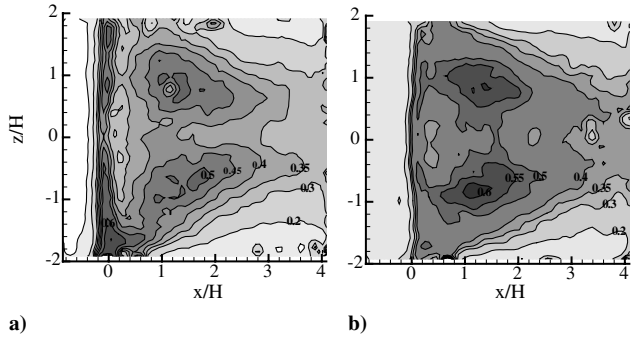

Fig. 15 Distribution of turbulence level in the spanwise plane for y/H of a) 0.16 and b) 0.32.

crossflow. The jet has a higher streamwise velocity near the side walls, likely caused by the increased deflection of the jet as the side walls are approached.

Figure 15 shows the distribution of the turbulence level defined similar to Eq. (3), although using the spanwise fluctuation w' instead of v'. The distributions are symmetric with respect to the spanwise center, with peaks located near $z/H \sim \pm 1$. Peak turbulence levels are located generally outside of the recirculation zone, although the boundary of the recirculation zone may extend into highly turbulent regions. Turbulent transport across the recirculation-zone boundary plays an important role in flame-holding dynamics within the recirculation zone, because unsteady flux of reactants and products across the boundary influences combustion rates and self-sustainability.

Although the recirculation zone is highly three-dimensional in nature, general dimensions of the recirculation zone in the midspan plane are of interest for global considerations related to the potential for flame anchoring. The height of the recirculation zone h is relatively simple to determine based on the peak of the trajectory of the streamline that originates from the downstream edge of the slot jet. Determining the length l is slightly more subjective, because of the bifurcating nature of the streamline that bounds the recirculation zone. The bifurcation is related to the downstream stagnation point of the recirculation zone illustrated in the spanwise streamline pattern (see Fig. 13) [50]. Figure 16 shows the length l and height h of the recirculation zone in the midspan plane as a function of MR. It is clear that the scale of the recirculation zone can be continuously controlled. The length of the recirculation zone begins to saturate at the higher-MR conditions, whereas the height shows less saturation at the higher-MR values. The effect of confinement is likely responsible for the saturation of the dimensions of the recirculation zone.

Figure 17 shows the integral length scale calculated as a function of the streamwise position for the low- and high-MR cases. The integral length scale is calculated from a transverse integration of the spatial correlation function based on the streamwise velocity fluctuations. The vertical reference point y/H at a given streamwise location x/H for the correlation function is coincident with the local peak turbulence level (i.e., the integral length scale is calculated on a

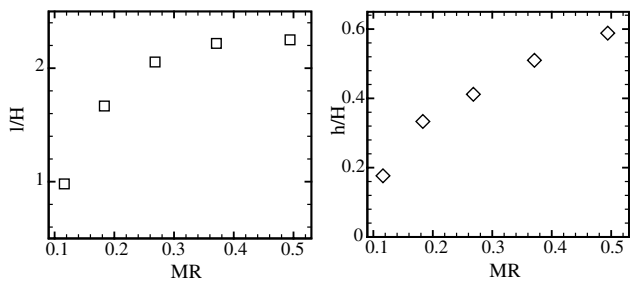

Fig. 16 Normalized a) length and b) height of the recirculation zone in the midspan plane as a function of MR.

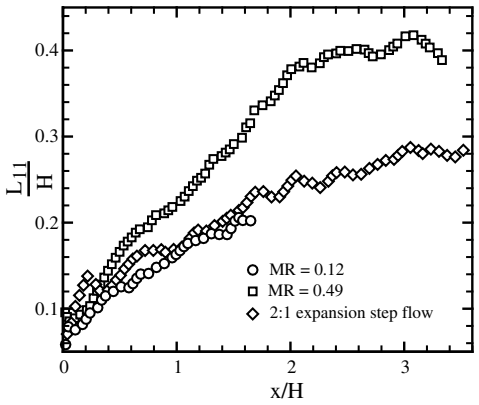

Fig. 17 Integral length scale as a function of streamwise position.

trajectory defined by the loci of peak turbulence level). The integral length scale calculated for the step flow is included in Fig. 17 for reference. It is clear that the transverse slot jet creates much larger-scale turbulence in comparison with the step flow. For combustion applications, this should be a benefit, because enhanced turbulent combustion should be realized [58]. The low-MR case produces scales that nearly match that of the step flow, even though the height of the recirculation zone is small relative to the step height for the rearward-facing step flow.

The ANSYS/CFX-10 calculations were done to complement the experimental data to provide further insight into the structure of the recirculation zone. A detailed quantitative validation of the computational fluid dynamics (CFD) was not undertaken, although it was found that the CFD provides qualitative agreement with the experimental data. Figure 18 shows the mean streamline pattern and mean streamwise velocity distribution for the CFD results in the midspan side-view plane for a MR of 0.49. The qualitative features of the flow are captured well by the CFD model (see the experimental data in Figs. 8b and 9b for comparison with Fig. 18). Figure 19 provides the CFD spanwise data at y/H of 0.16. The streamline pattern in the spanwise plane shows the same features as the experimental data. Now that the CFD results have been shown to represent the qualitative features of the flow, the numerical results can be used to help explain some of the observations of the three-dimensional flowfield. The level of agreement between the experiment and CFD results is surprising, although quantitative comparisons show that momentum diffusion is underpredicted by CFD. The qualitative agreement suggests that the flowfield mechanisms are robust and mainly governed by the boundary conditions and geometry.

Figure 20 presents the pressure coefficient distribution along the injection wall, with a reference pressure of 1 atm and normalized by

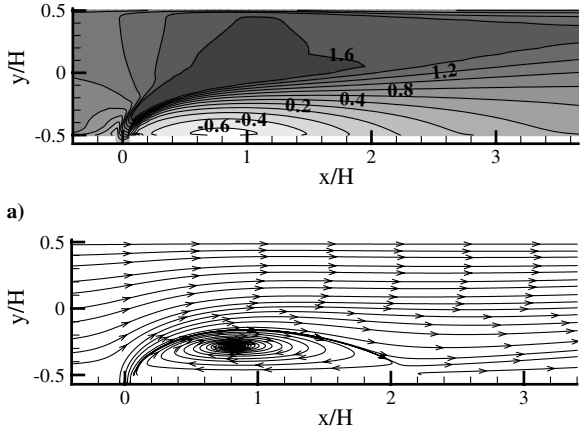

Fig. 18 Side-view midspan distribution of a) mean streamwise velocity and b) mean flow streamlines for the CFD model at MR = 0.49.

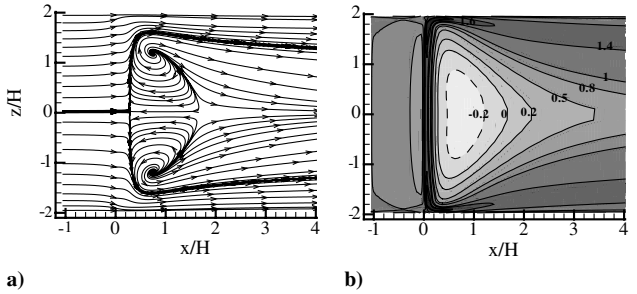

Fig. 19 Spanwise distribution of a) streamlines and b) mean streamwise velocity for the CFD model at MR = 0.49.

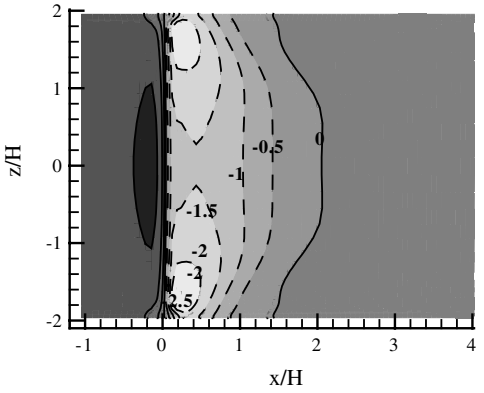

Fig. 20 Pressure coefficient distribution on the injection surface for the CFD model at MR = 0.49.

the dynamic pressure based on the characteristic channel velocity U_o. It is clear that the static pressure near the side walls and downstream of the injection-location region is a local minimum. The static pressure difference across the slot jet is a minimum near the midspan and increases toward the side walls. The higher pressure drop across the slot jet near the side walls produces a stronger deflection of the jet, resulting in the observed shorter-height recirculation region in this region. The jetlike flow that is created as the crossflow passes through the gap between the slot jet and the side walls likely creates this lower-pressure region due to the additional entrainment combined with the entrainment into the slot jet. The magnitude of this effect depends on the height of the recirculation zone, which is determined by the MR. At low MR, the flow near the center plane was found to be nominally two-dimensional (i.e., the mean flow satisfies two-dimensional mass continuity).

The DPIV results in the side and plan view have given an indication of the three-dimensional structure of the recirculation region. The ANSYS/CFX-10 model results provide a qualitative picture of the recirculation region. Figure 21 is a visualization of the CFD streamline pattern in the region downstream of the slot jet for both a 95 and 100% slot width. As identified in previous figures, the recirculation region for the 95% case has a triangular footprint and reaches a peak height in the midspan plane. Figure 21b shows that the recirculation zone for the 100% width slot jet is nominally two-dimensional, although side-wall effects create some weak spanwise variation. The 95% slot CFD results showed a CVP that emanated from the trailing edge of the recirculation zone. This CVP was not present in the 100% slot case. The grayscale contours represent mean streamwise velocity near the injection wall, with the 100% case showing strong spanwise uniformity.

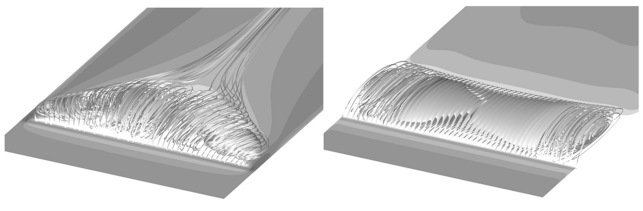

Fig. 21 CFD streamline pattern in the recirculation zone for the a) 95% and b) 100% slot jet at MR = 0.49.

IV. Conclusions

The current work explored the flowfield of the recirculation region generated using a transverse slot jet. The project is motivated by the desire to improve thrust performance of ramjet engines through reducing flow path losses, requiring a new strategy for flame-holding and turbulent-combustion enhancement. The current phase of the work focused on nonreacting flow to understand the basic turbulent flow features of the proposed configuration. A variety of momentum ratios were studied, ranging from zero to approximately 0.5. The slot spanned 95% of the channel duct, a feature that resulted in a highly three-dimensional mean flowfield. The longitudinal and transverse scales of the recirculation zone increase monotonically with momentum ratio. Comparisons were made to the flow downstream of a 2:1 area ratio rearward-facing step flow. It was found that the transverse slot jet produces high turbulence levels in a short streamwise distance, a trend that should benefit the targeted application. In addition to the enhanced turbulent energy, larger integral length scales were produced in the midspan plane compared with the step-flow results. A numerical aspect of the work employed CFD to model the qualitative characteristics of the flow. Static pressure distributions in the region of the slot exit provide an explanation for the observed domelike shape of the recirculation region. CFD calculations showed that a 100% slot case resulted in a nominally two-dimensional flowfield. Current studies are focused on flame holding and combustion rate measurements for the transverse slot jet for a crossflow containing a mixture of air and hydrocarbon fuels. The slot-to-channel depth ratio is considered a potentially important parameter for producing three-dimensionality and a CVP that might improve combustor performance compared with configurations that are two-dimensional. Future studies will also look at means for enhancing the CVP to determine if a strong CVP promotes enhanced combustion processes. Creating three-dimensional flow features will also contribute to the control of thermoacoustic instabilities; hence, the slot-to-channel depth ratio may be a parameter that influences unsteady combustion oscillations.

Acknowledgments

The authors would like to acknowledge the generous support of the Office of Naval Research under contract N00014-06-1-0498 as well as the guidance they have received from technical monitor Gabriel D. Roy. The authors appreciate the assistance from Jeremy Kruger, who participated in the rearward-facing step-flow experiments. The authors are also grateful to Praxair, Inc., for providing the ANSYS/CFX-10 licenses to the Department of Mechanical and Aerospace Engineering at the State University of New York at Buffalo.

References

[1] Andreopoulos, J., "On the Structure of Jets in a Crossflow," *Journal of Fluid Mechanics*, Vol. 157, Aug. 1985, pp. 163–197. doi:10.1017/S0022112085002348

[2] Andreopoulos, J., and Rodi, W., "Experimental Investigation of Jets in a Crossflow," *Journal of Fluid Mechanics*, Vol. 138, 1984, pp. 93–127. doi:10.1017/S0022112084000057

[3] Chassaing, P., George, J., Claria, A., and Sananes, F., "Physical Characteristics of Subsonic Jets in a Cross-Stream," *Journal of Fluid Mechanics*, Vol. 62, 1974, pp. 41–64. doi:10.1017/S0022112074000577

[4] Kamotani, Y., and Greber, I., "Experiments on a Turbulent Jet in a Cross Flow," *AIAA Journal*, Vol. 10, No. 11, 1972, pp. 1425–1429.

[5] Keffer, J., and Baines, W., "The Round Turbulent Jet in a Cross-Wind," *Journal of Fluid Mechanics*, Vol. 15, 1963, pp. 481–496. doi:10.1017/S0022112063000409

[6] Moussa, Z., Trischka, J., and Eskinazi, S., "The Near Field in the Mixing of a Round Jet with a Cross-Stream," *Journal of Fluid Mechanics*, Vol. 80, 1977, pp. 49–80. doi:10.1017/S0022112077001530

[7] Hasselbrink, E. F., and Mungal, M. G., "Transverse Jets and Jet Flames. Part 1. Scaling Laws for Strong Transverse Jets," *Journal of Fluid Mechanics*, Vol. 443, 2001, pp. 1–25. doi:10.1017/S0022112001005146

[8] Hasselbrink, E. F., and Mungal, M. G., "Transverse Jets and Jet Flames. Part 2. Velocity and Oh Field Imaging," *Journal of Fluid Mechanics*, Vol. 443, 2001, pp. 27–68. doi:10.1017/S0022112001005158

[9] Smith, S., and Mungal, M., "Mixing, Structure and Scaling of the Jet in Crossflow," *Journal of Fluid Mechanics*, Vol. 357, No. 01, 1998, pp. 83–122. doi:10.1017/S0022112097007891

[10] Yuan, L., Street, R., and Ferziger, J., "Large-Eddy Simulations of a Round Jet in Crossflow," *Journal of Fluid Mechanics*, Vol. 379, 1999, pp. 71–104. doi:10.1017/S0022112098003346

[11] Su, L., and Mungal, M., "Simultaneous Measurements of Scalar and Velocity Field Evolution in Turbulent Crossflowing Jets," *Journal of Fluid Mechanics*, Vol. 513, 2004, pp. 1–45. doi:10.1017/S0022112004009401

[12] Broadwell, J., and Breidenthal, R., "Structure and Mixing of a Transverse Jet in Incompressible Flow," *Journal of Fluid Mechanics*, Vol. 148, 1984, pp. 405–412. doi:10.1017/S0022112084002408

[13] Durando, N. A., "Vortices Induced in a Jet by a Subsonic Cross Flow," *AIAA Journal*, Vol. 9, No. 2, 1971, pp. 325–327.

[14] Karagozian, A. R., "An Analytical Model for the Vorticity Associated with a Transverse Jet," *AIAA Journal*, Vol. 24, No. 3, 1986, pp. 429–436.

[15] Coelho, S., and Hunt, J., "The Dynamics of the Near Field of Strong Jets in Crossflows," *Journal of Fluid Mechanics*, Vol. 200, 1989, pp. 95–120. doi:10.1017/S0022112089000583

[16] Fearn, R., and Weston, R. P., "Vorticity Associated With a Jet in a Cross Flow," *AIAA Journal*, Vol. 12, No. 12, 1974, pp. 1666–1671.

[17] Sykes, R., Lewellen, W., and Parker, S., "On the Vorticity Dynamics of a Turbulent Jet in a Crossflow," *Journal of Fluid Mechanics*, Vol. 168, 1986, pp. 393–413. doi:10.1017/S0022112086000435

[18] Cortelezzi, L., and Karagozian, A. R., "On the Formation of the Counter-Rotating Vortex Pair in Transverse Jets," *Journal of Fluid Mechanics*, Vol. 446, 2001, pp. 347–373.

[19] Fric, T., and Roshko, A., "Vortical Structure in the Wake of a Transverse Jet," *Journal of Fluid Mechanics*, Vol. 279, 1994, pp. 1–47. doi:10.1017/S0022112094003800

[20] Kelso, R., Lim, T., and Perry, A., "An Experimental Study of Round Jets in Cross-Flow," *Journal of Fluid Mechanics*, Vol. 306, 1996, pp. 111–144. doi:10.1017/S0022112096001255

[21] Kelso, R., and Smits, A., "Horseshoe Vortex Systems Resulting from the Interaction Between a Laminar Boundary Layer and a Transverse Jet," *Physics of Fluids*, Vol. 7, No. 1, 1995, pp. 153–158. doi:10.1063/1.868736

[22] Lim, T., New, T., and Luo, S., "On the Development of Large-Scale Structures of a Jet Normal to a Cross Flow," *Physics of Fluids*, Vol. 13, No. 3, 2001, pp. 770–775. doi:10.1063/1.1347960

[23] Shan, J., and Dimotakis, P., "Turbulent Mixing in Liquid-Phase Transverse Jets," Guggenheim Aeronautical Lab., California Inst. of Technology, Fluid Mechanics Rept. 2001.006, Pasadena, CA, 2001.

[24] Krothapalli, A., Lourenco, L., and Buchlin, J. M., "Separated Flow Upstream of a Jet in a Crossflow," *AIAA Journal*, Vol. 28, No. 3, 1990, pp. 414–420.

[25] McMahon, H., Hester, D., and Palfery, J., "Vortex Shedding from a Turbulent Jet in a Cross-Wind," *Journal of Fluid Mechanics*, Vol. 48, 1971, pp. 73–80. doi:10.1017/S0022112071001472

[26] New, T., Lim, T., and Luo, S., "Elliptic Jets in Cross-Flow," *Journal of Fluid Mechanics*, Vol. 494, 2003, pp. 119–140. doi:10.1017/S0022112003005925

[27] New, T., Lim, T., and Luo, S., "A Flow Field Study of an Elliptic Jet in Cross Flow Using DPIV Technique," *Experiments in Fluids*, Vol. 36, No. 4, 2004, pp. 604–618. doi:10.1007/s00348-003-0733-7

[28] Blanchard, J., Brunet, Y., and Merlen, A., "Influence of a Counter Rotating Vortex Pair on the Stability of a Jet in a Cross Flow: An Experimental Study by Flow Visualizations," *Experiments in Fluids*, Vol. 26, No. 1, 1999, pp. 63–74. doi:10.1007/s003480050265

[29] Haven, B., and Kurosaka, M., "Kidney and Anti-Kidney Vortices in Crossflow Jets," *Journal of Fluid Mechanics*, Vol. 352, 1997, pp. 27–64. doi:10.1017/S0022112097007271

[30] Holdeman, J. D., "Mixing of Multiple Jets with a Confined Subsonic Cross-Flow," *Progress in Energy and Combustion Science*, Vol. 19, No. 1, 1993, pp. 31–70. doi:10.1016/0360-1285(93)90021-6

[31] Jones, W., and Wille, M., "Large-Eddy Simulation of a Plane Jet in a Cross-Flow," *International Journal of Heat and Fluid Flow*, Vol. 17, No. 3, 1996, pp. 296–306. doi:10.1016/0142-727X(96)00045-8

[32] Kalita, K., "Prediction of Turbulent Plane Jet in Crossflow," *Numerical Heat Transfer, Part A, Applications*, Vol. 41, No. 1, 2002, pp. 101–111. doi:10.1080/104077802317221465

[33] Chen, K. S., and Hwang, J. Y., "Experimental Study on the Mixing of One- and Dual-Line Heated Jets with a Cold Crossflow in a Confined Channel," *AIAA Journal*, Vol. 29, No. 3, 1991, pp. 353–360.

[34] Haniu, H., and Ramaprian, B. R., "Studies on Two-Dimensional Curved Nonbuoyant Jets in Cross Flow," *Journal of Fluids Engineering*, Vol. 111, No. 1, 1989, pp. 78–86.

[35] Ramaprian, B. R., and Haniu, H., "Measurements in Two-Dimensional Plumes in Crossflow," *Journal of Fluids Engineering*, Vol. 111, No. 2, 1989, pp. 130–138.

[36] Plesniak, M., and Cusano, D., "Scalar Mixing in a Confined Rectangular Jet in Crossflow," *Journal of Fluid Mechanics*, Vol. 524, 2005, pp. 1–45. doi:10.1017/S0022112004001132

[37] Kalghatgi, G. T., "Blow-Out Stability of Gaseous Jet Diffusion Flames, 2: Effect of Cross Wind," *Combustion Science and Technology*, Vol. 26, Nos. 5–6, 1981, pp. 241–244. doi:10.1080/00102208108946965

[38] Ben-Yakar, A., and Hanson, R. K., "Cavity Flame-Holders for Ignition and Flame Stabilization in Scramjets: An Overview," *Journal of Propulsion and Power*, Vol. 17, No. 4, 2001, pp. 869–877.

[39] Takahashi, S., Sato, N., Tsue, M., Kono, M., Nakamura, M., Kondo, H., and Ujiie, Y., "Control of Flame-Holding in Supersonic Airflow by Secondary Air Injection," *Journal of Propulsion and Power*, Vol. 14, No. 1, 1998, pp. 18–23.

[40] Fry, R. S., "A Century of Ramjet Propulsion Technology Evolution," *Journal of Propulsion and Power*, Vol. 20, No. 1, 2004, pp. 27–58.

[41] Schadow, K. C., and Gutmark, E., "Combustion Instability Related to Vortex Shedding in Dump Combustors and Their Passive Control," *Progress in Energy and Combustion Science*, Vol. 18, No. 2, 1992, pp. 117–132. doi:10.1016/0360-1285(92)90020-2

[42] Schadow, K. C., Gutmark, E., Parr, T. P., Parr, D. M., Wilson, K. J., and Crump, J. E., "Large-Scale Coherent Structures as Drivers of Combustion Instability," *Combustion Science and Technology*, Vol. 64, Nos. 4–6, 1989, pp. 167–186. doi:10.1080/00102208908924029

[43] Gerbig, F., and Keady, P., "Size Distributions of Test Aerosols from a Laskin Nozzle," *Microcontamination*, Vol. 3, No. 7, July 1985, pp. 56–61.

[44] Lourenco, L., and Krothapalli, A., "True Resolution PIV: A Mesh-Free Second Order Accurate Algorithm," 10th International Symposium on Applications of Laser Techniques to Fluid Mechanics, Lisbon, Portugal, Calouste Gulbenkian Foundation, Paper 13.5, 2000.

[45] New, T., Lim, T., and Luo, S., "Effects of Jet Velocity Profiles on a Round Jet in Cross-Flow," *Experiments in Fluids*, Vol. 40, No. 6, 2006, pp. 859–875. doi:10.1007/s00348-006-0124-y

[46] Muppidi, S., and Mahesh, K., "Study of Trajectories of Jets in Crossflow Using Direct Numerical Simulations," *Journal of Fluid Mechanics*, Vol. 530, 2005, pp. 81–100. doi:10.1017/S0022112005003514

[47] Forliti, D. J., and Strykowski, P. J., "Controlling Turbulence in a Rearward-Facing Step Combustor Using Countercurrent Shear," *Journal of Fluids Engineering*, Vol. 127, No. 3, 2005, pp. 438–448. doi:10.1115/1.1899170

[48] Yuan, L., and Street, R., "Trajectory and Entrainment of a Round Jet in Crossflow," *Physics of Fluids*, Vol. 10, No. 9, 1998, pp. 2323–2335. doi:10.1063/1.869751

[49] Frolov, S., Basevich, V. Y., Belyaev, A. A., Posvianskii, V., and Radvogin, Y., "Modeling of Confined Flame Stabilization by Bluff

Bodies," *Advances in Chemical Propulsion*, CRC Press, Boca Raton, FL, 2001, pp. 191–214.

[50] Huang, R. F., and Hsieh, R. H., "Sectional Flow Structures in Near Wake of Elevated Jets in a Crossflow," *AIAA Journal*, Vol. 41, No. 8, 2003, pp. 1490–1499.

[51] Adams, E. W., and Johnston, J. P., "Effects of the Separating Shear-Layer on the Reattachment Flow Structure .2. Reattachment Length and Wall Shear-Stress," *Experiments in Fluids*, Vol. 6, No. 7, 1988, pp. 493–499.
doi:10.1007/BF00196511

[52] Behrens, A. A., Anderson, M. J., Strykowski, P. J., and Forliti, D. J., "Combustion Enhancement in a Dump Combustor Using Countercurrent Shear, Part 2: Heat Release Enhancement and Optimization," ASME International Mechanical Engineering Congress and Exposition, Orlando, FL, American Society of Mechanical Engineers Paper IMECE-2005-81267, 2005.

[53] Forliti, D. J., Behrens, A. A., Strykowski, P. J., and Tang, B. A., "Combustion Enhancement in a Dump Combustor Using Countercurrent Shear, Part 1: Nonreacting Flow Control and Preliminary Combustion Results," ASME International Mechanical Engineering Congress and Exposition, Orlando, FL, American Society of Mechanical Engineers Paper IMECE-2005-81274, 2005.

[54] Behrens, A. A., and Strykowski, P. J., "Controlling Volumetric Heat Release Rates in a Dump Combustor Using Countercurrent Shear," *AIAA Journal*, Vol. 45, No. 6, 2007, pp. 1317–1323.
doi:10.2514/1.24059

[55] Abdel-Gayed, R. G., Al-Khishali, K. J., and Bradley, D., "Turbulent Burning Velocities and Flame Straining in Explosions," *Proceedings of the Royal Society of London, Series A: Mathematical and Physical Sciences*, Vol. 391, No. 1801, 1984, pp. 393–414.

[56] Abdel-Gayed, R. G., Bradley, D., and Lawes, M., "Turbulent Burning Velocities: A General Correlation in Terms of Straining Rates," *Proceedings of the Royal Society of London, Series A: Mathematical and Physical Sciences*, Vol. 414, No. 1847, 1987, pp. 389–413.

[57] Poinsot, T., Veynante, D., and Candel, S., "Quenching Processes and Premixed Turbulent Combustion Diagrams," *Journal of Fluid Mechanics*, Vol. 228, 1991, pp. 561–606.

[58] Peters, N., "The Turbulent Burning Velocity for Large-Scale and Small-Scale Turbulence," *Journal of Fluid Mechanics*, Vol. 384, 1999, pp. 107–132.
doi:10.1017/S0022112098004212

J. Gore
Associate Editor